Hydrogen Electrooxidation under Conditions of High Mass Transport in Room Temperature Ionic Liquids and the Role of Underpotential-Deposited Hydrogen

*Sean E. Goodwin and Darren A. Walsh**

School of Chemistry, The University of Nottingham,

Nottingham NG7 2RD, UK

* darren.walsh@nottingham.ac.uk

Tel: +44 115 8467495; Fax: +44 115 9513562

Abstract

The hydrogen oxidation reaction (HOR), an electrocatalytic reaction of fundamental and applied interest, was studied in the protic ionic liquid (PIL) diethylmethylammonium trifluoromethanesulfonate, [dema][TfO], at Pt electrodes using rotating disk electrode (RDE) and ultramicroelectrode (UME) voltammetry. A steady-state HOR current is observed during RDE voltammetry at overpotentials > 50 mV but an additional plateau is observed in the overpotential region 50-200 mV when using UMEs. The difference in voltammetric responses is attributed to higher rate of mass transport to the UME than to the RDE. Three models have been used to fit the experimental data. The first is a dual-pathway model, which assumes that the Tafel-Volmer and Heyrovsky-Volmer pathways are both active over the potential range of interest and no blockage of catalytic sites occurs during the reaction. The second is a dual-pathway model, which assumes that reaction intermediates block access of H_2 to catalytic sites. The third is based on the premise that underpotential-deposited hydrogen atoms (H_{upd}) can block adsorption and electrooxidation of H_2 at the Pt surface. While each model fits the polarisation curves reasonably well, detailed analysis suggests that the H_{upd}-blocking model describes the responses better. To the best of our knowledge, this work is the first to demonstrate the advantages of UME voltammetry over RDE voltammetry for studying electrocatalytic reactions in PILs, and the first to show that H_{upd} can inhibit an electrocatalytic reactions in an ionic liquid, a factor that may become important as the technological applications of these liquids increase.

Introduction

The hydrogen oxidation reaction (HOR − Equation 1) is among the most important and widely studied of all electrochemical reactions. It is the anode reaction in proton exchange membrane fuel cells (PEMFCs)[1] and is often considered a prototype for electrocatalytic reactions, in which the rate of an electrochemical process depends on the identity of the electrode material.[2] The rate of the HOR can vary by as much as seven orders of magnitude when changing the electrode material from a poor electrocatalyst such as Hg to a good electrocatalyst such as Pt.[3]

$$H_2 \rightarrow 2H^+ + 2e^- \quad (1)$$

In part due to its importance in PEMFCs, and also due to the intriguing surface electrochemistry at play during the reaction, measurements of the mechanism and rate of the HOR in acidic and alkaline media have been carried out using Pt electrocatalysts for decades.[4-13] The Tafel-Heyrovsky-Volmer mechanism of the HOR in acidic medium contains three elementary steps:[14] the Tafel step (Equation 2) is the dissociative chemisorption of H_2 forming adsorbed H atoms (H_{ads}), the Heyrovsky step (Equation 3) is a chemical-electrochemical step involving both dissociative adsorption of H_2 to H_{ads} and ionisation to H^+, and the Volmer step (Equation 4) is oxidation of H_{ads}.

$$2Pt + H_2 \rightarrow 2PtH_{ads} \quad (2)$$

$$H_2 + Pt \rightarrow PtH_{ads} + H^+ + e^- \quad (3)$$

$$PtH_{ads} \rightarrow Pt + H^+ + e^- \quad (4)$$

By studying the kinetics of the HOR in various media, it is possible to differentiate between the dominant mechanisms that occur in different media or at different electrocatalyst surfaces. Perhaps the most widely-used method for studying HOR kinetics (and kinetics of the reverse reaction, the H_2-evolution reaction or HER) is RDE voltammetry. Exchange current densities, j_0 (the current density at zero overpotential), of the order of 1 mA cm^{-2} and Tafel slopes of about 30 mV $decade^{-1}$ have often been measured using Pt electrodes.[15-17] However, high-mass-transport methods such as UME voltammetry,[18] scanning electrochemical microscopy (SECM),[19] floating-electrode voltammetry,[20] and H_2-pumping methods[21,22] have yielded j_0 values in the range 20-80 mA cm^{-2},[21] in reasonable agreement with that suggested by the performance of PEMFC anodes.[23]

The adsorption of atomic hydrogen (often dubbed underpotential-deposited hydrogen, H_{upd}) onto Pt at potentials negative of 0.3 V *vs.* the reversible hydrogen electrode potential (Equation 5) is also of fundamental and applied interest to electrochemists. Studies of H_{upd} deposition on single-crystal Pt electrodes have revealed insights into the structure sensitivity of electrode reactions,[24] while measurement of the coverage of Pt electrodes by H_{upd} provides a means by which the electrochemically-active surface areas of Pt electrode surfaces can be determined.[25] It is also widely believed that H_{upd} deposition onto Pt can have a drastic effect on the HOR and, in this respect, there are two main views; the first is that H_{upd} is an intermediate in the HOR[18,26] and the second is that it is a spectator species that can hinder the HOR by blocking adsorption and activation of H_2.[17]

$$Pt + H^+ + e^- \rightarrow PtH_{upd} \quad (5)$$

Room temperature ionic liquids (RTILs) are materials that are composed entirely of ions and which are liquid below 100 °C (although we note that a proposal to increase the

temperature in this definition was recently published[27]).[28] Due to their unique properties, such as wide electrochemical windows, inherent conductivities, and thermal stabilities, the electrochemical applications of RTILs have increased significantly in recent years and include fundamental studies of mass- and charge-transfer dynamics,[29] and uses as electrolytes in devices such as fuel cells, batteries and supercapacitors.[30] Fundamental studies of electrocatalytic reactions in RTILs have also increased in number and include studies of the HOR.[30-32] For example, Compton has used aprotic ionic liquids (*i.e.*, those with aprotic organic cations) to reveal new insights into the roles of RTIL ions during the HOR (and HER) in RTILs.[33-36] The HOR has also been studied using protic ionic liquids (PILs), *i.e.*, RTILs formed by proton transfer from Brønsted acids to Brønsted bases,[32,37] in large part due to the realisation that PILs can be used as H^+-conducting electrolytes in intermediate-temperature, nonhumidified H_2 fuel cells, which can operate above the boiling point of water and so potentially offer more-efficient performances than conventional PEMFCs.[38-40] However, while it is known that adsorbates such as surface oxides can form in RTILs at positive potentials and affect the rate of the HOR[32] and other electrocatalytic processes,[32,41-43] it is unknown whether H_{upd}, which was only observed in RTILs for the first time recently,[44-46] plays any role. By exploring such phenomena using RTILs, it may be possible to gain new insights into the effects of the electrode/RTIL interfacial structure on electrocatalysis. Furthermore, an understanding of the effects of H_{upd} on electrocatalysis in RTILs may be technologically important in the future, particularly if we reach a point where high-performance, "task-specific" electrocatalysts and RTILs must be designed.

In this paper, we describe an electrochemical investigation into the rate and mechanism of the HOR in the PIL diethylmethylammonium trifluoromethanesulfonate, [dema][TfO] (Scheme 1). This particular PIL was chosen as it is the most promising PILs for use in nonhumidifed, PIL-based H_2-O_2 and H_2-Cl_2 fuel cells due to its relatively low viscosity,

high proton conductivity and thermal stability.[39,47] As we describe below, the HOR polarisation behaviour observed using RDE voltammetry differs significantly from that observed when using UMEs. During RDE voltammetry, the HOR current density reached a mass transport-limited value within about 50 mV of the HOR/HER equilibrium potential. By contrast, two distinct HOR plateaus were observed when using UMEs, and these plateaus were within the potential range in which H_{upd} can form on Pt in the PIL (~0.0 V-0.4 V). The difference in the UME and RDE voltammetry is attributed to the significant differences in the rates of mass transport to the UME and RDE surfaces; under the high mass-transport conditions at the UME, electron transfer kinetics dominated the response at potentials where the current was mass-transport limited at the RDE. As we describe below, good fits to the polarisation data were obtained using dual-pathway models in which the Tafel-Volmer and Heyrovsky-Volmer mechanism predominate in different potential regions[10] and another model in which H_{upd} acts as a blocking species,[18] but detailed analysis suggests that H_{upd}-blocking model is more applicable. To the best of our knowledge, this is the first time that the benefits of UME voltammetry over RDE voltammetry to measure the rates of fast electrochemical reactions have been demonstrated in RTILs and the first to demonstrate that H_{upd} plays a significant role during the HOR in RTILs.

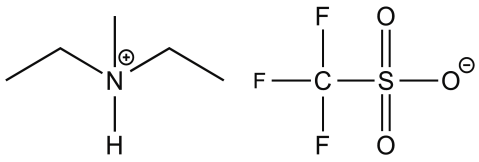

Scheme 1. *Structure of the protic ionic liquid diethylmethylammonium trifluroromethanesulfonate, [dema][TfO].*

Experimental Section

Materials and Apparatus. All reagents were from Alfa Aesar or Sigma-Aldrich and were used as received. [dema][TfO] was synthesised using the methods described in Reference 32 and, after drying under vacuum, contained < 200 ppm water. H_2 (99.995%), Ar (99.998%), and N_2 (99.998%) were from BOC gases (Nottingham, UK). Pt wire (25 μm diameter, 99.95% pure) was from Alfa Aesar. Electrochemical experiments were carried out using Model CHI910 and CHI760 potentiostats from CH Instruments (Austin, TX, USA). RDE voltammetry was performed using a Model MSR rotator and 5-mm diameter Pt disk RDE (Pine Instruments, Grove City, PA, USA).

Fabrication of Ultramicroelectrodes. Pt UMEs with nominal diameters of 25 μm were fabricated using the method described in Reference 48. Briefly, a short section of 25-μm diameter Pt wire was sealed into borosilicate glass using a resistive coil to collapse the glass. Electrical contact was then made to the open end of the Pt wire and the sealed end was exposed by grinding and polishing to reveal a Pt disk inlaid in glass. Disk-shaped, Pt-in-quartz UMEs with diameters in the range 1.4-3.0 μm were fabricated using the laser-puller method described in Reference 49. Prior to use, the Pt RDE and 25 μm-diameter UMEs were cleaned by polishing with 0.05-μm alumina slurry (Buehler, Lake Bluff, IL, USA) on a felt polishing pad, rinsed with deionised water, and dried under N_2. The Pt-in-quartz UMEs were cleaned by rinsing with ultra-pure water and then holding briefly in a butane flame until the Pt glowed bright yellow.

Electrochemical Measurements. A three-electrode electrochemical cell containing either the Pt RDE or UME working electrode and a Pt flag counter electrode (A = 0.45 cm^2) was used for electrochemical measurements. The reference electrode was a Hydroflex reversible hydrogen electrode from Gaskatel (Kassel, Germany), which consists of H_2 flowing over a platinised gas-diffusion electrode and provides a stable potential in PILs.[45] The

potential of the Hydroflex electrode is the same as that obtained by flowing H_2 over a Pt flag in the PIL, as introduced by Watanabe for electrochemical measurements in PILs, and the equilibrium potential, E_{eq}, for the HOR/HER reactions is 0.0 V in a cell containing H_2-saturated [dema][TfO], a Pt working electrode and Pt flag RHE.[39] All potentials are reported as overpotentials ($\eta = E - E_{eq}$). All currents were normalised to the surface areas of the electrodes and expressed as current densities, j. Prior to performing HOR measurements, the Pt electrodes were activated in the PIL by scanning the potential between 0.0 V and 2.0 V at 50 mV s^{-1} until unchanging CVs were recorded. During HOR measurements, potential sweeps were started at the positive potential limit to ensure that a freshly-reduced surface was formed, before H_{upd} deposited negative of ~400 mV.

Results and Discussion

HOR Electrooxidation in [dema][TfO]. Figure 1A shows an RDE voltammogram recorded in blank [dema][TfO]. The general shape of the voltammogram is similar to that observed during cyclic voltammetry of polycrystalline Pt in acidic media, and to that reported previously for voltammetry of Pt in RTILs containing trace water.[42,45] An oxidation wave appeared at $\eta > 1.0$ V due to oxidation of the Pt surface in the presence of the trace water that is ubiquitous in ionic liquids.[42] Between approximately 0.4 V and 0.0 V, H_{upd} (from reduction of protons in the PIL) formed on the surface[45] during the negative sweep and was oxidised during the positive sweep according to Equation 5. At negative potentials, the cathodic HER current flowed. Figure 1B show the voltammograms recorded in H_2-saturated [dema][TfO] at a range of electrode rotation rates, ω. The general shape of the voltammograms agrees with that recorded previously by Angell and co-workers using PILs;[37] the low HOR current above 1.0 V was due to the presence of the adsorbed oxide layer, which blocked electrocatalysis of the HOR. A mass-transport-limited HOR current appeared between approximately 0.05 V and

0.6-0.8 V, and the HOR current decreased rapidly from 0.05 V to 0.00 V before the cathodic HER current started to flow at negative potentials. From the data shown in Figure 1, it is clear that the HOR proceeded in the PIL in the potential region in which H_{upd} was present on the Pt surface.

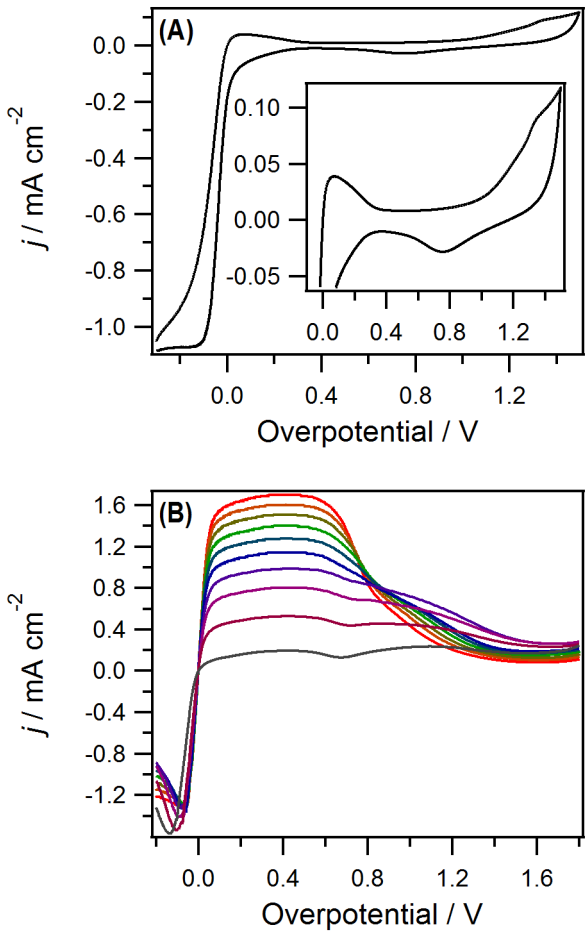

Figure 1. *(A) iR-corrected RDE voltammogram recorded at a 5-mm diameter Pt RDE in Ar-saturated [dema][TfO] rotating at 1,800 rpm by cycling the potential between −0.3 V (initial potential) and 1.5 V at 50 mV* s^{-1}*. The inset shows the same voltammogram in the potential region > 0.0 V. (B) iR-corrected RDE voltammograms recorded in* H_2*-saturated [dema][TfO] by sweeping the potential from 1.8 V to −0.2 V at 50 mV* s^{-1}*. The RDE was rotated at rotation rates between 0 rpm (grey line) and 1,800 rpm (red line) in 200 rpm intervals.*

Figure 2A shows the low overpotential region (0.0 V to 0.4 V) of the RDE data shown in Figure 1B but, in this case, the j values have been normalised to the limiting currents, j_{lim}. The normalised sweeps overlap extremely well, showing that changing the mass-transport dynamics of the system resulted in normalised polarisation curves with the same shapes. By contrast, Figure 2B shows plots of j/j_{lim}, but, in this case, the data were recorded at UMEs with differing radii, r. There was a clear change in the shape of the normalised curves as r decreased; two plateaus became visible and j_{lim} was reached at more positive potentials. The plateau observed at low potentials at the 1.4 μm UME (green line in Figure 2B) is not as clear as that recorded at the 3 μm UME but plateaus can be discerned at the UMEs between about 0.05-0.15 V, while the limiting currents measured at each UME do not meet until about 0.4 V.

The appearance of additional features during HOR voltammetry at the UMEs can be attributed to an increase in mass transport to the UME over that observed at the RDE.[18] For a disk UME, the mass-transport coefficient, m is ~D/r. The diffusion coefficient of H_2 in the PIL, D_{H_2}, was determined to be 8.7×10^{-6} cm^2 s^{-1} (see below for details), so m ~0.02 cm s^{-1} for the 3 μm-radius UME in [dema][TfO]. In the case of an RDE, m is given by:

$$m = 0.62 D^{\frac{2}{3}} \nu^{-\frac{1}{6}} \omega^{\frac{1}{2}} \quad (6)$$

where ν is the kinematic viscosity of the solvent. To achieve m = 0.02 cm s^{-1} at the RDE during the HOR in [dema][TfO], the required ω would be > 5×10^5 rpm, which is impractical due to the cavitation effects that occur near RDE surfaces at such rates.[50] Therefore, by carrying out the HOR at such small UMEs, the reaction was under kinetic control at the UME in the potential region where it is diffusion controlled at the RDE.

Dual-Pathway HOR Model without Site-Blocking Effects. Adzic[10] and Chialvo[51,52] have both developed dual-pathway kinetic models that predict the existence of a shoulder or

plateau in the HOR polarisation curves at low overpotentials, prior to a larger limiting current at higher overpotentials. These models were developed to fit data previously recorded by Kucernak[18] using a series of differently-sized Pt UMEs in H_2-saturated 0.5 M H_2SO_4. In these models, the rate constants of the individual reaction steps increase in the order $k_{Heyrovsky} < k_{Tafel} < k_{Volmer}$. If we consider first the Tafel-Volmer mechanism (Equations 2 and 4,

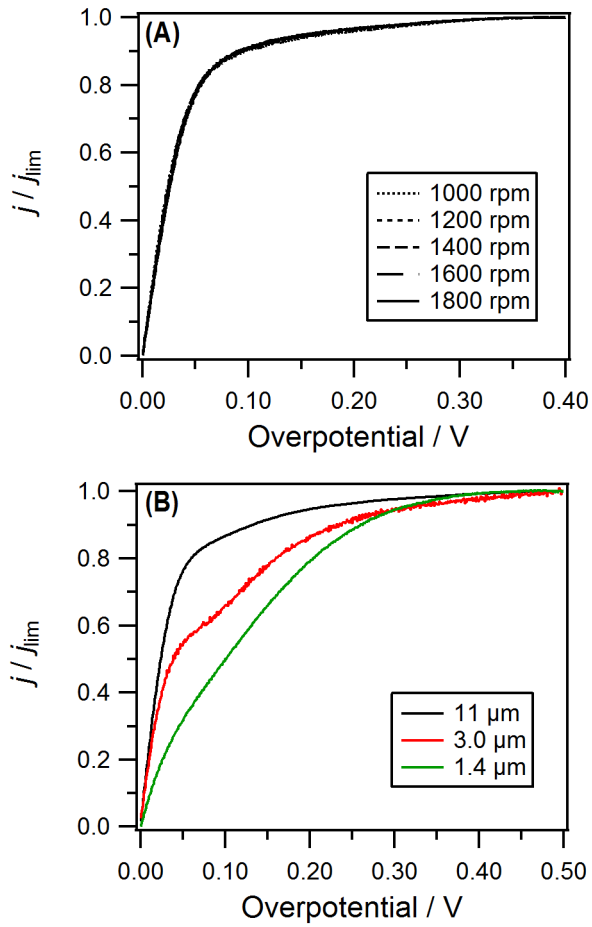

Figure 2. *(A) iR-corrected RDE voltammograms recorded in H_2-saturated [dema][TfO] at a 5-mm diameter Pt RDE as the potential was swept from 1.8 V to −0.2 V at 50 mV s^{-1} at a range of rotation rates. Current densities have been divided by j_{lim} of the corresponding voltammogram. (B) Linear sweep voltammograms recorded at 50 mV s^{-1} (except for that recorded at the 3.0 µm radius UME, which was done at 10 mV s^{-1}) in H_2-saturated [dema][TfO] at Pt UMEs of various radii. Potentials were swept in negative direction and UMEs were pre-anodized at 2.0 V prior to the experiment.*

respectively), the Tafel step is independent of applied potential and the first plateau in the voltammograms is then the limiting current due to the Tafel-Volmer pathway. At low overpotentials, the Heyrovsky-Volmer pathway contributes negligibly to the overall current but, as the overpotential increases, the rate of Heyrovksy-Volmer pathway (Equations 3 and 4, respectively) increases, resulting in the current increase positive of the first plateau. The second plateau at higher overpotentials is then the mass-transport limited current when the rate of the Heyrovksy-Volmer mechanism plus that of the Tafel-Volmer mechanism becomes greater than the rate of mass transport of H_2 to the electrode. In the model described by Adzic, it is assumed that Butler-Volmer kinetics apply for the Volmer and Heyrovsky steps and that concentration polarisation of the protonated species is negligible. The degree of concentration polarisation of H_2 between the surface, c_{H_2}, and the bulk, $c^0_{H_2}$, is expressed by Equation 7 and Equation 8 then gives the normalised rate of the HOR as a function of η:[10]

$$\frac{c_{H_2}}{c^0_{H_2}} = \left(1 - \frac{j}{j_{lim}}\right) \tag{7}$$

$$\frac{j}{j_{lim}} = \frac{\dfrac{2F\upsilon_{0T}\left[\left(\dfrac{1-\theta}{1-\theta^0}\right)^2 - \left(\dfrac{\theta}{\theta^0}\right)^2\right] + 2F\upsilon_{0H}\left[\left(\dfrac{1-\theta}{1-\theta^0}\right)\exp\left(\dfrac{F\eta}{2RT}\right) - \left(\dfrac{\theta}{\theta^0}\right)\exp\left(\dfrac{-F\eta}{2RT}\right)\right]}{1 + \left[2F\upsilon_{0T}\left(\dfrac{1-\theta}{1-\theta^0}\right)^2 + 2F\upsilon_{0H}\left(\dfrac{1-\theta}{1-\theta^0}\right)\exp\left(\dfrac{F\eta}{2RT}\right)\right] / j_L}}{j_{lim}} = \frac{\dfrac{j_f - j_b}{1 + \dfrac{j_f}{j_{lim}}}}{j_{lim}} \tag{8}$$

where F is the Faraday constant, R is the universal gas constant, and T is the absolute temperature. The constants υ_{0T}, υ_{0H}, and υ_{0V} are exchange current densities for each mechanistic step, but expressed in units of mol s^{-1} cm^{-2} (multiplying υ_{0H} by F gives the more

familiar j_{0H}, or exchange current density of the Heyrovsky step in A cm^{-2}). The right side of Equation 8 is included to explain what the middle term represents, where j_f and j_b are the current densities corresponding to the forward and back reactions, respectively. For an unrestricted surface coverage of H_{ads}, θ, the potential-dependent coverage is given by:

$$\frac{\theta}{\theta^0} = \frac{\exp\left(-\frac{F\eta}{\gamma RT}\right)}{1-\theta^0+\theta^0\exp\left(\frac{F\eta}{\gamma RT}\right)} \tag{9}$$

where θ^0 is the H_{ads} coverage at equilibrium and γ is determined by the relative exchange rates of the elementary processes. If one ignores any potential site-blocking effects of the intermediate H_{ads}, Equation 10 is obtained:

$$\frac{j}{j_{lim}} = \frac{\frac{S\left[j_{0T}\left(1-\exp\left(\frac{-2F\eta}{\gamma RT}\right)\right)+j_{0H}\left(\exp\left(\frac{F\eta}{2RT}\right)-\exp\left(\frac{-F\eta}{\gamma RT}\right)\exp\left(\frac{-F\eta}{2RT}\right)\right)\right]}{j_{lim}}}{1+\frac{S\left(j_{0T}+j_{0H}\exp\left(\frac{F\eta}{2RT}\right)\right)}{j_{lim}}} = \frac{\frac{j_f-j_b}{j_{lim}}}{1+\frac{j_f}{j_{lim}}} \tag{10}$$

where j_{0T} is the exchange current density of the Tafel step. Aside from ignoring site-blocking effects, the difference between Equations 8 and 10 is that the concentration polarization of H_2 between the electrode surface and the bulk electrolyte, and the surface roughness of the electrode, are incorporated into the dimensionless parameter S in Equation 10. In addition, reaction rates are expressed as j_0 values instead of υ_0 values. For a more detailed derivation of Equation 10, the reader is directed to Reference 10.

We have fitted curves generated using Equation 10 to experimental normalised HOR polarisation curves and the resulting fits are shown in Figure 3. In agreement with the approach taken in Reference 10, we have kept $S = 1$ and found that attempts to fit the data with a single j_{0T} value across all electrode sizes resulted in poor fits. In addition, varying j_{0H} did not contribute significantly to the overall quality of the fits, and so the quality of the fits was primarily a result of varying j_{0T} and γ. j_{0V} was determined from the best-fit values of γ, j_{0T} and j_{0H} using Equation 11 and the best-fit parameters are shown in Table 1.

$$j_{0V} = \frac{4 j_{0T} + j_{0H}(\gamma + 1)}{\gamma - 1} \tag{11}$$

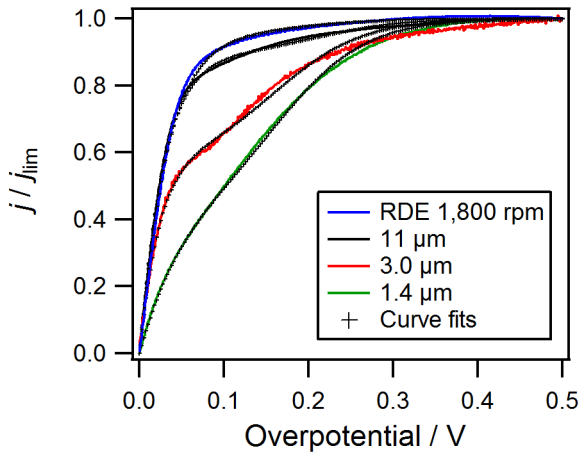

Figure 3. *Theoretical fits (markers) to the experimental data recorded in H_2-saturated [dema][TfO] at 3 UMEs (radii given by legend) and an RDE sweep at 1,800 rpm. Potentials were swept in negative direction from 1.8 V at 50 mV s^{-1}, except for the 3.0-µm radius electrode, which was swept at 10 mV s^{-1}. Electrodes were pre-activated by potential cycling to 2.0 V before the negative sweep. Theoretical curves were generated using Equation 10 in the text and best-fit parameters are given in Table 1.*

Table 1. *Best-fit kinetic parameters for the HOR obtained from the fits in Figure 3.*

Size	j_{0T} (mA cm^{-2})	j_{0H} (mA cm^{-2})	γ	j_{0V} (mA cm^{-2})
RDE	33.1	0.97	2.6	84.3
11	48.3	0.95	2.2	162.1
3.4	12.6	0.96	1.8	62.6
1.4	11.4	0.96	3.0	24.9

While the agreement between the experimental data and calculated curves is quite good in general, there is some disagreement at high overpotentials, in particular for the data obtained using the 3.0 μm-radius UME. It is also clear from the fitting parameters that there is some disagreement in the best-fit terms. j_{0T} varied from 11 to 48 mA cm^{-2} as r increased (note that this is a change in an apparent exchange current density, assuming that the Volmer step is the fast step, as the Tafel step does not itself involve electron transfer), while j_{0V} varied by more than a factor of 6. Such fitting issues notwithstanding, we note that the best-fit values increased in the order $j_{0H} < j_{0T} < j_{0V}$, as expected. In addition, and even though the response was under kinetic control over a very small potential region, we have fitted our data recorded using RDE voltammetry to Equation 10 and found that the quality of the fit was quite good and the best-fit values agreed quite well with those determined from the UME data (blue line in Figure 3 and Table 1), giving us additional confidence in our extracted values. The parameter γ is a function of the rates of the different steps of the HOR and our best-fit values are generally slightly higher than for the HOR in aqueous media, indicating that the rate constants of the three steps of the HOR are closer in value to one another than in aqueous media.[10]

Dual-Pathway HOR Model incorporating Site-Blocking Effects. We also investigated the quality of the fits achievable when site-blocking effects are incorporated into the model. Such effects will be important because, unless the surface coverage of H_{ads} is

negligible at any given time, then H_{ads} will block sites that would otherwise be available for H_2 adsorption. Note that H_{ads} refers to the HOR reaction intermediate; this model does not consider H_{upd} adsorption. Incorporation of site-blocking effects into the model gives Equation 12:[10]

$$\frac{j}{j_{lim}} = \frac{S\left[j_{0T}(1-\theta)^2 + j_{0H}(1-\theta)\exp\left(\frac{F\eta}{2RT}\right)\right] - S\left[j_{0T}(1-\theta^0)^2\left(\frac{\theta}{\theta^0}\right)^2 + j_{0H}(1-\theta^0)\left(\frac{\theta}{\theta^0}\right)\exp\left(\frac{-F\eta}{2RT}\right)\right]}{1 + \frac{S\left[j_{0T}(1-\theta)^2 + j_{0H}(1-\theta)\exp\left(\frac{F\eta}{2RT}\right)\right]}{j_{lim}}} \Big/ j_{lim} \qquad (12)$$

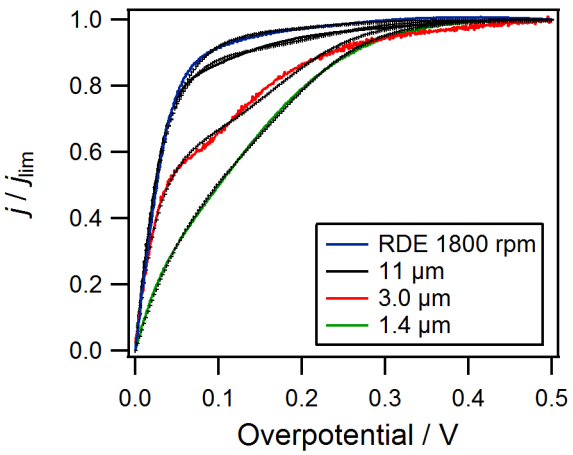

Figure 4: *Theoretical fits (crosses) to the experimental data recorded in H_2-saturated [dema][TfO] at 3 UMEs (radii given by legend) and one RDE sweep at 1,800 rpm. Potentials were swept in negative direction from 1.8 V at 50 mV s^{-1}, except for at the 3.0 µm-radius electrode, which was swept 10 mV s^{-1}. Electrodes were pre-activated by potential cycling to 2.0 V. Theoretical curves were generated using Equations 12 in the text and best-fit parameters are given in Table 2.*

Table 2. *Best-fit parameters obtained from the fits shown in Figure 4.*

Size	j_{0T} (mA cm^{-2})	j_{0H} (mA cm^{-2})	θ^0	γ	j_{0V} (mA cm^{-2})
RDE	41.1	0.63	0.005	2.6	102.9
11	51.2	0.86	0.005	2.2	167.7
3.4	14.1	0.87	0.005	2.0	58.9
1.4	20.4	0.82	0.005	3.0	42.4

A new set of fitted curves were generated using Equation 12 and are shown in Figure 4. As the fitted θ^0 decreased, variation in the other parameters also decreased, suggesting that θ^0 was low. The best-fit parameters (Table 2) obtained by holding θ^0 at 0.005 show a small but significant improvement over the data in Table 1 with regards to the scatter of the j_{0T} values. However, the scatter of the j_{0V} values has not improved over that of the best-fit values obtained using the non-site-blocking model.

Single-Pathway HOR Model incorporating Blocking of Surface Sites by H_{upd}. It has been proposed that H_{upd} should not hinder the HOR in aqueous media as the H_{ads} intermediate occupies atop adsorption sites whereas H_{upd} occupies multifold adsorption sites.[10] However, others have suggested that H_{upd} is a spectator that may block adsorption and reaction of H_2 by altering the electronic properties of the electrocatalyst and/or by hindering adsorption of H_{ads}.[8,17] Kucernak has pointed out that the formation of H_{upd} (Equation 5) is basically the reverse of the Volmer step (Equation 4), if one ignores the difference between H_{upd} and H_{ads}.[18] It was posited that any sites available for H_{ads} formation should also be available to H_{upd} (formed in the absence of dissolved H_2) and, based on this premise, a single-pathway model for the HOR that does not take into account any difference between H_{upd} and H_{ads} was developed. Remarkably, the model also showed two plateaus in the HOR polarisation curves and fits to experimental polarisation curves were good at low potentials but less so at higher

potentials.[18] Adzic's non-site-blocking model fitted the data much better suggesting that a dual-pathway model, described the HOR in aqueous media better.[10] In agreement with the assumption inherent in the dual-pathway models described above, Kucernak's model was built on the premise that oxidation of H at Pt is the fast reaction step (at least in aqueous media), so irrespective of the operative mechanism (Tafel-Volmer or Heyrovsky-Volmer), dissociative adsorption of H_2 is rate determining.[18] Dissociation of H_2 requires free Pt sites (no difference between H_{upd} and H_{ads} is assumed), *i.e.*, free from H_{upd}, and the rate of the HOR is then a function of both overpotential and H_{upd} coverage:

$$\frac{j}{j_{\lim}} = \frac{1 - \exp\left(\frac{-2F\eta}{RT}\right)}{1 + \frac{j_{\lim}}{\sum\left[j_{0,i}\frac{(\theta_i^* - \theta_i)^{m_r}}{(\theta_i^* - \theta_i^0)^{m_r}}\exp\left(\gamma_i f_i\left(\theta_i - \theta_i^0\right)\right)\right]}\exp - \left(\frac{(2 - m_r)\beta F\eta}{RT}\right)} \tag{13}$$

where θ_i^* is the saturation coverage of H_{upd}, θ_i is the H_{upd} coverage at η, θ_i^0 is the H_{upd} coverage at equilibrium, γ is a symmetry factor for H_{ads}-H_{upd} interaction and f is the energy of this interaction (assuming a Frumkin adsorption isotherm), β is the electron transfer coefficient and m_r = 2 or 1 for the Tafel-Volmer or Heyrovsky-Volmer mechanism, respectively. The contributions of two different forms of H_{upd} (the strongly-bound, H_{SB}, and weakly-bound, H_{WB} forms) are considered, and i represents these two different forms. In order to use Equation 13, the coverage of H_{upd} as a function of overpotential in our PIL had to be known and in Figure 5 we have deconvoluted the H_{upd} region into H_{SB} and H_{WB} sites, which give the parameter θ in Equation 13. As very little is currently known about H_{upd} adsorption in PILs, the curve fits were deliberately kept as simple as possible, allowing only

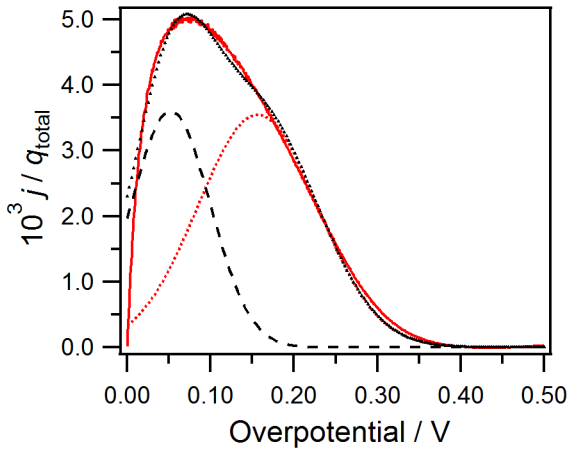

Figure 5: *Fitting theoretical H_{upd} to experimental H_{upd} data. Experimental data were recorded using a 5 mm diameter Pt RDE rotating at 1,800 rpm while the potential was swept at 50 mVs^{-1} in Ar-saturated [dema][TfO]. The vertical axis scale (current density) has been normalised to the integrated charge under the H_{upd} peaks (giving units of cm^{-2} s^{-1}). The experimental curve is the solid red line. The best-fit H_{WB} curve is shown in by the dashed line. The best-fit H_{SB} curve is the red dotted line and the total fitted H_{upd} curve is shown by the solid black line.*

two peaks with normal distributions. Interestingly, reasonable fits could only be obtained by allowing proton adsorption to continue negative of 0.0 V (dashed line in Figure 5), as also observed in $HClO_4$ (aq)[8] and H_2SO_4 (aq).[26] Additionally, the H_{upd} coverage (measured by integrating the charge under the H_{upd} oxidation peaks) observed in [dema][TfO] was only about 20% of that observed at the same electrode in an aqueous media, suggesting that competitive adsorption of the PIL ions onto the Pt surface may have occurred in the liquid. While it has been shown that $[TfO]^-$ ions do not adsorb onto Pt electrodes from aqueous media,[53] recent work using CO displacement has shown that PIL ions can adsorb onto Pt.[45] However, such work is in its infancy and the effects of the applied potential on adsorption of ions remains relatively poorly understood. Consequently, in this work we have ignored competitive PIL adsorption in our models and, indeed, by using the H_{upd} coverages obtained

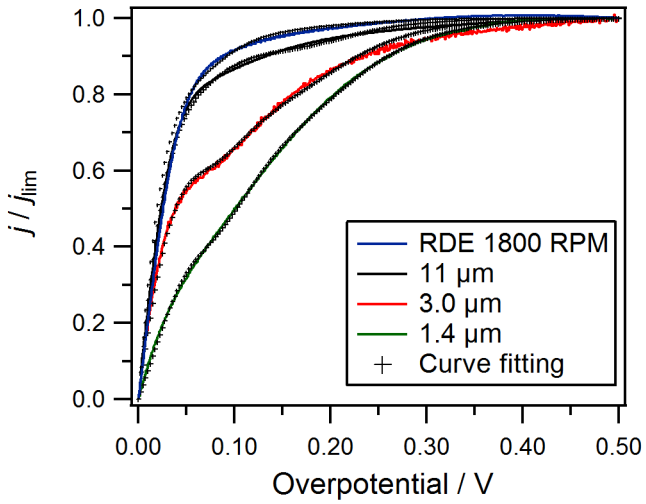

Figure 6. *Theoretical fits (markers) to the experimental data recorded in H_2 saturated [dema][TfO] at 3 UMEs (radii given by legend) and one RDE sweep at 1,800 rpm. Potentials were swept in negative direction from 1.8 V at 50 mV s^{-1}, except for the 3.0 µm radius electrode, which was swept 10 mV s^{-1}. Electrodes were pre-activated by potential cycling to 2.0 V. Theoretical curves were generated using Equation 13 in the text and best-fit parameters are given in Table 3.*

from the fits in Figure 5, the fits to the data generated from Equation 13 are very good (Figure 6). Again, and despite the fact that the response was under kinetic control over a very small potential region, we have fitted our data recorded using RDE voltammetry to Equation 13 and found that the quality of the fit was quite good and the best-fit values agreed quite well with those determined from the UME data. As with the dual pathway model, the saturation coverage of H_{upd} was fixed and the other parameters were allowed to vary. A number of combinations of θ^0 values were tested, and the tabulated values gave the closest fits and the agreement between the best-fit parameters obtained using each set of UME data was quite good. While these values of θ^0 show that about 1/5 of the electrode is covered with H_{upd} at equilibrium, Figure 5 shows that the weakly bound sites should have a greater coverage of H_{upd} than the strongly bound sites at equilibrium. The opposite is observed in the fitting

Table 3. *Best-fit parameters obtained using the fits shown in Figure 6.*

r / μm	θ^0 (WB)	θ^0 (SB)	j_0 (WB) (mA cm^{-2})	j_0 (SB) (mA cm^{-2})	γf (WB)	γf (SB)	Electron Transfer Coefficient
1.4	0.037	0.187	1.6	1.3	8.7	5.5	0.46
3.0	0.037	0.187	3.3	1.4	10.0	7.0	0.46
11	0.037	0.187	2.9	3.9	8.0	9.0	0.46
250 (RDE)	0.037	0.187	1.2	2.5	9	4.5	0.46

parameters, and reasonable fits cannot be obtained by reversing these numbers. This suggests that the simple model that we have used to fit our H_{upd} envelope is deficient. To truly understand these effects and understand the coverage of H_{SB} and H_{WB} with applied potential at Pt in ionic liquids, it is likely that electrochemical measurements must be performed using single-crystal electrodes, an area of research that is just developing.[54]

Curve fits were attempted using values of $m_r = 2$ and 1, and by far the best fits were obtained when $m_r = 1$. This corresponds to the Heyrovsky-Volmer mechanism (Equations 3 and 4), which we note is the same as that determined for the HER at Pt in a number of aprotic RTILs based on the bis(trifluoromethanesulfonyl)imide anion.[44] We also note that our values of γf are positive, which indicates that there was an attractive interaction between adsorbates on the Pt surface.

Comparison of HOR Models. From the quality of the curve fits, it is not obvious which of the preceding models best describes the HOR in the PIL. However, we note that if the HOR proceeds *via* the dual pathway kinetic model in Equation 8, then at overpotentials close to the equilibrium potential the Tafel-Volmer mechanism should predominate (as $j_{0H} <$

j_{0T}). The Tafel-Volmer mechanism involves an electron transfer preceded by a chemical step (a so-called CE mechanism). It has been argued that if this mechanism is dominant then the current-overpotential relationship should be similar to that of a mass-transport limited response, but in which the current is limited by the chemical step (hydrogen dissociation) and not the rate of mass transport. In this instance a plot of η versus $-\ln(1-j/j_{lim})$ should yield a straight line according to Equation 14:[18]

$$\eta = -\frac{RT}{nF}\ln\left(1-\frac{j}{j_{lim}}\right) \quad (14)$$

Figure 7 shows such plots for the data recorded at each UME and, at the largest UME, the plot deviates clearly from a straight line, while that recorded using the smaller UMEs approach linearity. However, the gradient of the line obtained using the smallest UME is 182 mV, considerably higher than the theoretical values given by RT/nF (13 mV, with $n = 2$). In fact, it is the largest UME that yielded the gradient closest to the theoretical gradient (33 mV when $0 \leq \eta \leq 50$ mV), but it is the data recorded using this UME that deviates most significantly from a straight line. Finally, the gradients of all the UMEs should be equal to each other, but are not. This tells us that it is unlikely that the rate of reaction at low overpotentials is limited only by a preceding chemical step, suggesting that the Heyrovsky mechanism was active at low (<100 mV) overpotentials. We also tested the H_{upd}-blocking model to see if the Tafel-Volmer mechanism was dominant at low overpotentials. At very low overpotentials, Equation 13 simplifies to Equation 15, in much the same way that the Butler-Volmer equation (which is clearly inapplicable to our data) can be linearised in the "micropolarisation" region:[17,55]

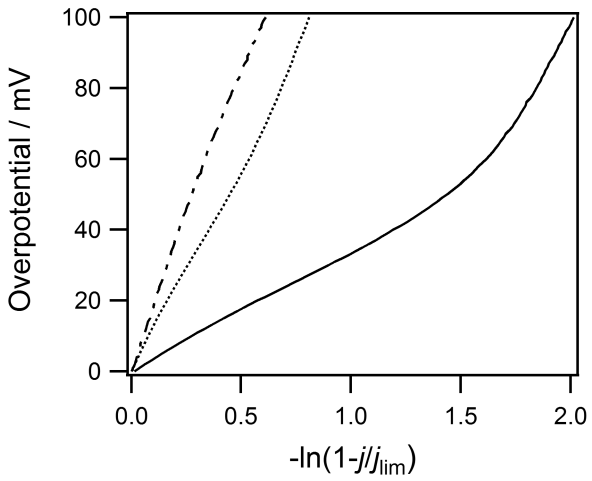

Figure 7*. Plots of overpotential vs -ln(1-j/j_{lim}) for the HOR in H_2 saturated [dema][TfO]. Curves are shown for Pt UMEs of radii 11 μm (solid line), 3.0 μm (dotted line) and 1.4 μm (dot-dashed line).*

$$j = \frac{\frac{2F}{RT}\eta}{\frac{1}{j_{\text{lim}}} + \frac{1}{j_0}} \tag{15}$$

Equation 15 is only valid if the Tafel-Volmer mechanism is dominant. If the Heyrovsky-Volmer mechanism was active at low overpotentials then m_r = 1 and Equation 13 cannot be simplified to a linear form. While the micropolarisation regions shown in Figure 8 are linear, consideration of Equation 15 shows that the gradients should increase with decreasing r (as j_{lim} increases with decreasing r). This is not the case, with the 3.0-μm radius UME data showing the steepest gradient. Therefore, it does appear unlikely that the Tafel-Volmer mechanism was the dominant reaction pathway at low overpotentials, in agreement with the data extracted from Figure 6.

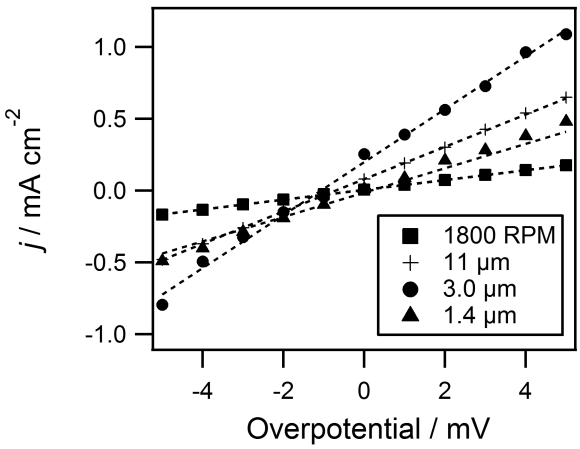

Figure 8. *Linear sweep voltammogram , only showing potentials 5 mV positive and negative of the HOR/HER equilibrium. Symbols: negative going potential sweep of Pt UMEs and Pt RDE (0.5 cm diameter, 1,800rpm) in H_2 saturated [dema][TfO] at 25 °C. Scan rates at 50 mV s^{-1} except 3.0 µm at 10 mV s^{-1}. Electrodes pre-activated by potential cycling to 2.0 V. Dashed lines are lines of best fit.*

HOR Exchange Current Densities and Rate Constants. While it is clear that the fits in Figures 3, 4 and 6 are all reasonable, the higher degree of variation in the best-fit kinetic parameters from the dual-pathway models (Tables 1 and 2) and the analysis at the end of the last section suggest that the H_{upd}-blocking model fits the HOR polarisation in the PIL better. It is notable that the H_{upd}-blocking model yielded significantly-lower j_0 values than the dual-pathway models. As described in the Introduction, studies of electrocatalytic processes in RTILs have only appeared in recent years and very few of those have addressed the HOR and HER so there are very little data to which we can compare our extracted kinetic parameters. Meng and Compton reported standard rate constants, $k^{0,}$ for the HER (from dissolved protons) in the range 10^{-3}-10^{-8} cm s^{-1} (depending on the composition of the electrocatalyst surface) in a series of aprotic RTILs.[36] In addition, Zhang studied the HER in a series of aprotic RTILs and calculated k^0 values of the order of 10^{-4} cm s^{-1},[44] but there is no such data reported for the

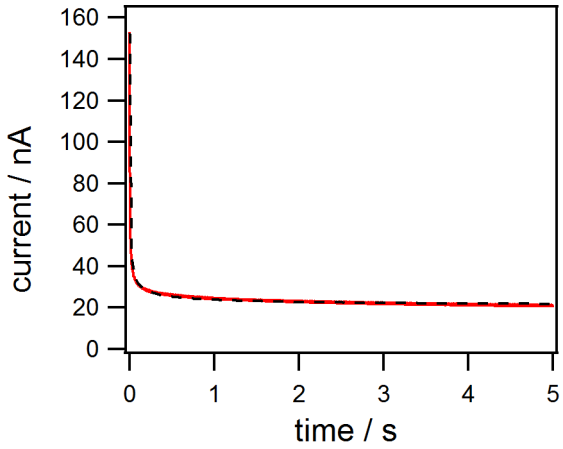

Figure 9. *HOR Chronoamperogram recorded by stepping the potential of a 14 μm-radius Pt UME from 0 V to 0.26 V in H_2-saturated [dema][TfO] at 25 °C*

HER (or HOR) in PILs. To convert our j_0 values to k^0 values knowledge of the saturation concentration, C_{H_2}, of H_2 in [dema][TfO] is required. C_{H_2} and D_{H_2} were determined using potential-step chronoamperometry at a UME and Figure 9 shows the current-time (i–t) transient recorded in the in H_2-saturated PIL by stepping the potential from one where the HOR did not occur to one where the HOR occurred at the diffusion-controlled rate. The dashed line in Figure 9 shows the fit to the data generated using the Shoup-Szabo expression:

$$i = \frac{4nFAD_{H_2}C_{H_2}}{\pi r} f(t) \qquad (16)$$

where $f(t)$ and τ are given by Equations 17 and 18:

$$f(t) = 0.7854 + 0.8862\tau^{-\frac{1}{2}} + 0.2146e^{(-0.7823\tau^{-\frac{1}{2}})} \qquad (17)$$

$$\tau = \frac{4D_{H_2}t}{r^2} \quad (18)$$

From the best-fit of Equation 16 (which Figure 9 shows was an excellent fit) to the experimental data, values of $D_{H_2} = 8.7 \times 10^{-6}$ cm^2 s^{-1} and $C_{H_2} = 2.1$ mM were obtained. j_0 was then converted to k^0 using Equation 19:

$$j_0 = 2Fk^0C_{H_2} \quad (19)$$

Using Equation 19, k^0 was determined to be ~0.01 cm s^{-1}, which is orders of magnitude larger than that determined for the HER in aprotic RTILs. While the observation of a relatively-fast HOR rate at Pt in PILs is encouraging for the developing of devices such as PIL-based H_2 fuel cells, it is notable that the O_2 reduction reaction in PILs is more complicated and slower.[43,56] It is our opinion that detailed kinetic analyses such as that described herein will help not only with the development and discovery of new, high-performance electrocatalysts for use in such media but will also aid in understanding the fundamental electrochemistry of these novel media.

Conclusions

Two current plateaus have been observed in the normalized voltammograms recorded during ultramicroelectrode voltammetry of the H_2 oxidation reaction in H_2-saturated diethylmethylammonium trifluoromethansulfonate, [dema][TfO]. This phenomenon became apparent during ultramicroelectrode voltammetry but not during rotating disk electrode voltammetry due to more-efficient mass transport to the ultramicroelectrode surface. Three

models have been used to explain the observations: two dual pathway kinetic models that do and do not incorporate the effects of site-blocking by reaction intermediates, and another that treats underpotential-deposited H atoms as a species that blocks electrocatalytic sites during the reaction. While each model gave very good fits to the experimental data, there was a significant difference in the kinetic parameters determined using each. By treating the Tafel-Volmer mechanism of H_2 oxidation as involving a preceding chemical step, and considering the chemical step to be analogous to a diffusion-limited step, we determined that the Tafel-Volmer mechanism was not the only pathway active at low overpotentials (< 100 mV). Given this observation, and the extremely good fits of the underpotential-deposited H inhibition model with our experimental data, we conclude that underpotential-deposited H atoms most likely act as blocking intermediate during the reaction in the ionic liquid. The observations that underpotential-deposited H atoms are stable during electrocatalysis in an ionic liquid is interesting and adds to our knowledge of these unique electrolytes and may well aid to those researchers interested in developing new electrocatalysts for H_2 electrooxidation in these unique media.

Acknowledgements

We thank the EPSRC Centre for Doctoral Training in Fuel Cells and their Fuels for SG's studentship.

References

(1) Wee, J. H.; Lee, K. Y. Overview of the Development of CO-tolerant Anode Electrocatalysts for Proton-Exchange Membrane Fuel Cells. *J. Power Sources* **2006**, *157*, 128-135.

(2) Santos, E.; Potting, K.; Schmickler, W. On the Catalysis of the Hydrogen Oxidation. *Faraday Discuss.* **2009**, *140*, 209-218.

(3) Li, H.; Lee, K.; Zhang, J. L. In *PEM Fuel Cell Electrocatalysts and Catalyst Layers: Fundamentals and Applications*; Zhang, J. L., Ed.; Springer-Verlag: London, 2008.

(4) Strmcnik, D.; Uchimura, M.; Wang, C.; Subbaraman, R.; Danilovic, N.; van der, V.; Paulikas, A. P.; Stamenkovic, V. R.; Marković, N. M. Improving the Hydrogen Oxidation Reaction Rate by Promotion of Hydroxyl Adsorption. *Nat. Chem.* **2013**, *5*, 300-306.

(5) Greeley, J.; Marković, N. M. The Road from Animal Electricity to Green Energy: Combining Experiment and Theory in Electrocatalysis. *Energy Environ. Sci.* **2012**, *5*, 9246-9256.

(6) Uchida, H.; Izumi, K.; Aoki, K.; Watanabe, M. Temperature-dependence of Hydrogen Oxidation Reaction Rates and CO-tolerance at Carbon-supported Pt, Pt-Co, and Pt-Ru Catalysts. *Phys. Chem. Chem. Phys.* **2009**, *11*, 1771-1779.

(7) Kucernak, A. R.; Toyoda, E. Studying the Oxygen Reduction and Hydrogen Oxidation Reactions under Realistic Fuel Cell Conditions. *Electrochem. Commun.* **2008**, *10*, 1728-1731.

(8) Strmcnik, D.; Tripkovic, D.; van der Vliet, D.; Stamenkovic, V.; Marković, N. M. Adsorption of Hydrogen on Pt(111) and Pt(100) Surfaces and its Role in the HOR. *Electrochem. Commun.* **2008**, *10*, 1602-1605.

(9) Mello, R. M. Q.; Ticianelli, E. A. Kinetic Study of the Hydrogen Oxidation Reaction on Platinum and Nafion® Covered Platinum Electrodes. *Electrochim. Acta* **1997**, *42*, 1031-1039.

(10) Wang, J. X.; Springer, T. E.; Adzic, R. R. Dual-Pathway Kinetic Equation for the Hydrogen Oxidation Reaction on Pt Electrodes. *J. Electrochem. Soc.* **2006**, *153*, A1732-A1740.

(11) Couturier, G.; Kirk, D. W.; Hyde, P. J.; Srinivasan, S. Electrocatalysis of the Hydrogen Oxidation and of the Oxygen Reduction Reactions of Pt and some Alloys in Alkaline Medium. *Electrochim. Acta* **1987**, *32*, 995-1005.

(12) Lin, C.; Jiao, X.; Tschulik, K.; Batchelor-McAuley, C.; Compton, R. G. Influence of Adsorption Kinetics upon the Electrochemically Reversible Hydrogen Oxidation Reaction. *J. Phys. Chem. C* **2015**, *119*, 16121-16130.

(13) Durst, J.; Siebel, A.; Simon, C.; Hasche, F.; Herranz, J.; Gasteiger, H. A. New Insights into the Electrochemical Hydrogen Oxidation and Evolution Reaction Mechanism. *Energy Environ. Sci.* **2014**, *7*, 2255-2260.

(14) Compton, R. G.; Banks, C. E. *Understanding Voltammetry*; 2nd ed.; Imperial College Press: London, 2011.

(15) Kita, H.; Ye, S.; Gao, Y. Mass-transfer Effect in Hydrogen Evolution Reaction on Pt Single-Crystal Electrodes in Acid-solution. *J. Electroanal. Chem.* **1992**, *334*, 351-357.

(16) Maruyama, J.; Inaba, M.; Katakura, K.; Ogumi, Z.; Takehara, Z. Influence of Nafion® Film on the Kinetics of Anodic Hydrogen Oxidation. *J.Electroanal. Chem.* **1998**, *447*, 201-209.

(17) Marković, N. M.; Grgur, B. N.; Ross, P. N. Temperature-dependent Hydrogen Electrochemistry on Platinum Low-index Single-crystal Surfaces in Acid Solutions. *J. Phys. Chem. B* **1997**, *101*, 5405-5413.

(18) Chen, S. L.; Kucernak, A. Electrocatalysis under Conditions of High Mass Transport: Investigation of Hydrogen Oxidation on Single Submicron Pt Particles Supported on Carbon. *J. Phys. Chem. B* **2004**, *108*, 13984-13994.

(19) Zhou, J.; Zu, Y.; Bard, A. J. Scanning Electrochemical Microscopy: Part 39. The Proton/Hydrogen Mediator System and its Application to the Study of the Electrocatalysis of Hydrogen Oxidation. *J. Electroanal. Chem.* **2000**, *491*, 22-29.

(20) Zalitis, C. M.; Kramer, D.; Kucernak, A. R. Electrocatalytic Performance of Fuel Cell Reactions at Low Catalyst Loading and High Mass Transport. *Phys. Chem. Chem. Phys.* **2013**, *15*, 4329-4340.

(21) Durst, J.; Simon, C.; Hasché, F.; Gasteiger, H. A. Hydrogen Oxidation and Evolution Reaction Kinetics on Carbon Supported Pt, Ir, Rh, and Pd Electrocatalysts in Acidic Media. *J. Electrochem. Soc.* **2015**, *162*, F190-F203.

(22) Neyerlin, K. C.; Gu, W.; Jorne, J.; Gasteiger, H. A. Study of the Exchange Current Density for the Hydrogen Oxidation and Evolution Reactions. *J. Electrochem. Soc.* **2007**, *154*, B631-B635.

(23) Gasteiger, H. A.; Panels, J. E.; Yan, S. G. Dependence of PEM Fuel Cell Performance on Catalyst Loading. *J. Power Sources* **2004**, *127*, 162-171.

(24) Marković, N. M.; Ross, P. N. Surface Science Studies of Model Fuel Cell Electrocatalysts. *Surf. Sci. Rep.* **2002**, *45*, 121-229.

(25) Trasatti, S.; Petrii, O. A. Real Surface-area Measurement in Electrochemistry. *Pure Appl. Chem.* **1991**, *63*, 711-734.

(26) Conway, B. E.; Tilak, B. V. Interfacial Processes involving Electrocatalytic Evolution and Oxidation of H_2, and the Role of Chemisorbed H. *Electrochim. Acta* **2002**, *47*, 3571-3594.

(27) Fletcher, S.; Black, V.; Kirkpatrick, I.; Varley, T. Quantum Design of Ionic Liquids for Extreme Chemical Inertness and a New Theory of the Glass Transition. *J. Solid State Electrochem.* **2013**, *17*, 327-337.

(28) Angell, C. A.; Byrne, N.; Belieres, J. P. Parallel Developments in Aprotic and Protic Ionic Liquids: Physical Chemistry and Applications. *Acc. Chem. Res.* **2007**, *40*, 1228-1236.

(29) Walsh, D. A.; Lovelock, K. R. J.; Licence, P. Ultramicroelectrode Voltammetry and Scanning Electrochemical Microscopy in Room-temperature Ionic Liquid Electrolytes. *Chem. Soc. Rev.* **2010**, *39*, 4185-4194.

(30) MacFarlane, D. R.; Tachikawa, N.; Forsyth, M.; Pringle, J. M.; Howlett, P. C.; Elliott, G. D.; Davis, J. H.; Watanabe, M.; Simon, P.; Angell, C. A. Energy Applications of Ionic Liquids. *Energy Environ. Sci.* **2014**, *7*, 232-250.

(31) Barrosse-Antle, L. E.; Bond, A. M.; Compton, R. G.; O'Mahony, A. M.; Rogers, E. I.; Silvester, D. S. Voltammetry in Room Temperature Ionic Liquids: Comparisons and Contrasts with Conventional Electrochemical Solvents. *Chem. Asian J.* **2010**, *5*, 202-230.

(32) Johnson, L.; Ejigu, A.; Licence, P.; Walsh, D. A. Hydrogen Oxidation and Oxygen Reduction in Protic Ionic Liquids. *J. Phys. Chem. C* **2012**, *116*, 18048-18056.

(33) Silvester, D. S.; Ward, K. R.; Aldous, L.; Hardacre, C.; Compton, R. G. The Electrochemical Oxidation of Hydrogen at Activated Platinum Electrodes in Room Temperature Ionic liquids as Solvents. *J. Electroanal. Chem.* **2008**, *618*, 53-60.

(34) Silvester, D. S.; Aldous, L.; Hardacre, C.; Compton, R. G. An Electrochemical Study of the Oxidation of Hydrogen at Platinum Electrodes in Several Room Temperature Ionic Liquids. *J. Phys. Chem. B* **2007**, *111*, 5000-5007.

(35) Meng, Y.; Aldous, L.; Belding, S. R.; Compton, R. G. The Formal Potentials and Electrode Kinetics of the Proton/Hydrogen Couple in Various Room Temperature Ionic Liquids. *Chem. Commun.* **2012**, *48*, 5572-5574.

(36) Meng, Y.; Aldous, L.; Belding, S. R.; Compton, R. G. The Hydrogen Evolution Reaction in a Room Temperature Ionic Liquid: Mechanism and Electrocatalyst Trends. *Phys. Chem. Chem. Phys.* **2012**, *14*, 5222-5228.

(37) Bautista-Martinez, J. A.; Tang, L.; Belieres, J. P.; Zeller, R.; Angell, C. A.; Friesen, C. Hydrogen Redox in Protic Ionic Liquids and a Direct Measurement of Proton Thermodynamics. *J. Phys. Chem. C* **2009**, *113*, 12586-12593.

(38) Belieres, J.-P.; Gervasio, D.; Angell, C. A. Binary Inorganic Salt Mixtures as High Conductivity Liquid Electrolytes for > 100 Degrees C Fuel Cells. *Chem. Commun.* **2006**, 4799-4801.

(39) Lee, S.-Y.; Ogawa, A.; Kanno, M.; Nakamoto, H.; Yasuda, T.; Watanabe, M. Nonhumidified Intermediate Temperature Fuel Cells Using Protic Ionic Liquids. *J. Am. Chem. Soc.* **2010**, *132*, 9764-9773.

(40) Díaz, M.; Ortiz, A.; Ortiz, I. Progress in the Use of Ionic Liquids as Electrolyte Membranes in Fuel Cells. *J. Membr. Sci.* **2014**, *469*, 379-396.

(41) Ejigu, A.; Johnson, L.; Licence, P.; Walsh, D. A. Electrocatalytic Oxidation of Methanol and Carbon Monoxide at Platinum in Protic Ionic Liquids. *Electrochem. Commun.* **2012**, *23*, 122-124.

(42) Walsh, D. A.; Ejigu, A.; Muhammad, S.; Licence, P. The Formation and Role of Oxide Layers on Pt during Hydrazine Oxidation in Protic Ionic Liquids. *ChemElectroChem* **2014**, *1*, 281-288.

(43) Walsh, D. A.; Ejigu, A.; Smith, J.; Licence, P. Kinetics and Mechanism of Oxygen Reduction in a Protic Ionic Liquid. *Phys. Chem. Chem. Phys.* **2013**, *15*, 7548-7554.

(44) Bentley, C. L.; Bond, A. M.; Hollenkamp, A. F.; Mahon, P. J.; Zhang, J. Mass Transport Studies and Hydrogen Evolution at a Platinum Electrode Using

Bis(trifluoromethanesulfonyl)imide as the Proton Source in Ionic Liquids and Conventional Solvents. *J. Phys. Chem. C* **2014**, *118*, 29663-29673.

(45) Ejigu, A.; Walsh, D. A. The Role of Adsorbed Ions during Electrocatalysis in Ionic Liquids. *J. Phys. Chem. C* **2014**, *118*, 7414-7422.

(46) Meng, Y.; Norman, S.; Hardacre, C.; Compton, R. G. The Electroreduction of Benzoic Acid: Voltammetric Observation of Adsorbed Hydrogen at a Platinum Microelectrode in Room Temperature Ionic Liquids. *Phys. Chem. Chem. Phys.* **2013**, *15*, 2031-2036.

(47) Liu, S.; Zhou, L.; Wang, P.; Zhang, F.; Yu, S.; Shao, Z.; Yi, B. Ionic-Liquid-Based Proton Conducting Membranes for Anhydrous H_2/Cl_2 Fuel-Cell Applications. *ACS. Appl. Mater. Interfaces* **2014**, *6*, 3195-3200.

(48) Zoski, C. G. Ultramicroelectrodes: Design, Fabrication, and Characterization. *Electroanalysis* **2002**, *14*, 1041-1051.

(49) Lovelock, K. R. J.; Cowling, F. N.; Taylor, A. W.; Licence, P.; Walsh, D. A. Effect of Viscosity on Steady-State Voltammetry and Scanning Electrochemical Microscopy in Room Temperature Ionic Liquids. *J. Phys. Chem.* **2010**, *13*, 4442-4450.

(50) Zhao, C.; Burrell, G.; Torriero, A. A. J.; Separovic, F.; Dunlop, N. F.; MacFarlane, D. R.; Bond, A. M. Electrochemistry of Room Temperature Protic Ionic Liquids. *J. Phys. Chem. B* **2008**, *112*, 6923-6936.

(51) Quaino, P. M.; Fernández, J. L.; Gennero de Chialvo, M. R.; Chialvo, A. C. Hydrogen Oxidation Reaction on Microelectrodes: Analysis of the Contribution of the Kinetic Routes. *J. Mol. Catal. A: Chemical* **2006**, *252*, 156-162.

(52) Gennero de Chialvo, M. R.; Chialvo, A. C. Hydrogen Diffusion Effects on the Kinetics of the Hydrogen Electrode Reaction. Part I. Theoretical Aspects. *Phys. Chem. Chem. Phys.* **2004**, *6*, 4009-4017.

(53) Berna, A.; Feliu, J. M.; Gancs, L.; Mukerjee, S. Voltammetric Characterization of Pt Single Crystal Electrodes with Basal Orientations in Trifluoromethanesulphonic Acid. *Electrochem. Commun.* **2008**, *10*, 1695-1698.

(54) Hanc-Scherer, F. A.; Sánchez-Sánchez, C. M.; Ilea, P.; Herrero, E. Surface-Sensitive Electrooxidation of Carbon Monoxide in Room Temperature Ionic Liquids. *ACS Catal.* **2013**, *3*, 2935-2938.

(55) Bard, A. J.; Faulkner, L. R. *Electrochemical Methods: Fundamentals and Applications*; 2nd ed.; John Wiley & Sons: New York, 2001.

(56) Khan, A.; Lu, X.; Aldous, L.; Zhao, C. Oxygen Reduction Reaction in Room Temperature Protic Ionic Liquids. *J. Phys. Chem. C* **2013**, *117*, 18334-18342.